Optics & Laser Technology 180 (2025) 111502

Contents lists available at ScienceDirect

Optics and Laser Technology

journal homepage: www.elsevier.com/locate/optlastec

Full length article

A nonlinear model of flexoelectric liquid crystal diffraction gratings

Qihao Han, Steve J. Elston, Waqas Kamal, Linpei Xue, Stephen M. Morris *

Department of Engineering Science, University of Oxford, Parks Road, Oxford OX1 3PJ, UK

ARTICLE INFO

Keywords:
Nematic liquid crystal
Flexoelectric effect
Nonlinear model
Numerical simulation
Diffraction grating

ABSTRACT

This paper presents a nonlinear model for flexoelectric liquid crystal (LC) diffraction gratings and compares the results from simulations with those obtained from experiments, providing a more accurate description of the behaviour of the flexoelectric LC grating than that offered by the linear models that have been considered previously. The nonlinear model that is constructed considers both dielectric and flexoelectric coupling and, with the aid of numerical simulations, enables the visualization of the behaviour of the LC director in response to flexoelectric, dielectric, and elastic effects. From the numerical simulations, both in-plane and out-of-plane tilt angles are obtained which are then used to simulate the optical wave propagation and diffraction characteristics for light passing through the LC flexoelectric grating. To compare the results from simulations with experiments, we develop an LC mixture that is capable of forming a flexoelectric LC diffraction grating at room temperature. This mixture allows for real-time manipulation of the periodic splay-bend structure by adjusting the amplitude of the DC electric field, enabling control of the diffraction angle and intensity of light into the different diffraction orders. The consistency observed between our simulation results and experimental data underscores the reliability and accuracy of our proposed models.

1. Introduction

Liquid crystals (LC) are an excellent example of functional materials with notable electro-optical characteristics due to their significant optical anisotropy and pronounced responsiveness to external stimuli, including electric fields [1]. These functional materials have been studied and deployed in a range of applications spanning different fields in consumer electronics and device engineering; the most obvious example being their widespread success in flat panel display technology. Besides displays, their unique ability to modulate light [2–5] makes them particularly appealing for beam steering technology [5–9], switchable holograms [10–12], and other uses of intensity and phase modulation [13–15]. Tunable LC diffraction gratings are a key component for beam-steering applications as they are cost-effective, lightweight, and consume low power [16,17]. Most importantly, they can facilitate real-time modification of the diffraction, aligning with the dynamic requirements of modern optical applications.

In the fabrication of tunable LC gratings, nematic LCs, which are characterized by an absence of an inherent macroscopic periodic structure, have proven to be especially popular. A widely adopted technique employed to induce a diffraction grating in a nematic LC is to apply a periodic electric field across the LC layer, which can be achieved with patterned electrodes [10,18,19]. Alternatively, to avoid the need for patterned electrodes, the LC director can be spatially patterned using photoalignment layers in combination with ultraviolet (UV) light and photomasks [20–22]. The process of patterning the alignment layer, however, can be complex, which can increase the cost and time involved in manufacturing. Additionally, the morphology of the resulting diffraction grating can be inherently limited, confining its capacity to diffract light to a limited range of angles.

Chiral nematic LCs, characterized by their intrinsic macroscopic periodic helical structure, have also been explored for use as tunable diffraction gratings [23–26]. In this case, the grating properties can be controlled by adjusting the concentration of the chiral dopant, and consequently the pitch, and the applied electric field [25,26]. However, a significant constraint with such systems is the lack of control of the diffraction efficiency and the slow response time which is typically of the order of several seconds [27].

The flexoelectric effect in nematic LCs, which was predicted by Meyer in 1969 [28], offers a potential route to the realisation of tunable LC gratings. For certain molecules with a shape asymmetry, splay and bend deformations can induce a net polarization within the material. Conversely, the application of an electric field can result in the formation of a macroscopic splay-bend deformation [29]. The flexoelectric

* Corresponding author.
E-mail addresses: qihao.han@eng.ox.ac.uk (Q. Han), stephen.morris@eng.ox.ac.uk (S.M. Morris).

https://doi.org/10.1016/j.optlastec.2024.111502
Received 18 June 2024; Accepted 18 July 2024
Available online 6 August 2024

free energy (f_{flexo}) equation characterizes the coupling between the flexoelectric polarization $\mathbf{P}_{\text{flexo}} = e_1\mathbf{n}(\nabla \bullet \mathbf{n}) + e_3(\nabla \times \mathbf{n}) \times \mathbf{n}$ (e_1 and e_3 represent the splay and bend flexoelectric coefficient, respectively) and the applied electrical field $\mathbf{E}$, which can be expressed as $f_{flexo} = -\mathbf{E} \bullet \mathbf{P}_{\text{flexo}}$. Recent studies have demonstrated the possibility of forming tunable diffraction gratings using the flexoelectric effect in bent-core LCs [30–32]. However, such studies have not considered in detail the role of dielectric coupling and how this will suppress the desired periodic structure, adversely impacting the diffraction grating. Furthermore, bent-core molecules do not typically exist in the nematic phase at room temperatures.

Modelling flexoelectric LC diffraction gratings plays a crucial role in predicting, analyzing, and visualizing the behaviour of the LC director. Towards this end, Bobylev and Pikin proposed a theoretical model that employs the small angle approximation for linearizing the LC director, and used an Euler-Lagrange approach to minimize the total free energy equation [33]. This model accurately clarified the threshold conditions required to trigger the flexoelectric effect. However, their analysis did not extend to the role of dielectric anisotropy ($\Delta\varepsilon$) on the overall director profile. Additionally, the equations that were presented are only applicable under certain threshold conditions and do not necessarily hold in more general situations. Separately, Shin proposed a conical model that assumes the alignment of the LC director is arranged within a cone [34]. Through the computation of the average free energy density, aimed at the optimal minimization of the total free energy, this methodology can be used to precisely calculate the periodicity of the flexoelectric undulations. Nevertheless, the conical model that was proposed does not sufficiently consider the impact of dielectric coupling and is thus unable to provide an accurate simulation of the LC director profile when both flexoelectric and dielectric coupling needs to be accounted for.

In this paper, we present both modelling and experimental investigations of flexoelectric-based LC diffraction gratings taking into account both flexoelectric and dielectric coupling. Regarding the modelling aspects, we employ both linear and nonlinear models in both the unconstrained and constrained (conical) coordinate systems to investigate the LC behaviour in the presence of flexoelectric and dielectric coupling. For the experiments, we present results for a nematic LC mixture that is capable of forming diffraction gratings at room temperature under direct current (DC) conditions. We then check whether the grating can dynamically tune the diffraction angle and efficiency when a laser beam passes through it. The comparison between our experimental findings and the outcomes of our simulations shows the reliability and validity of our proposed nonlinear model.

2. Theoretical modelling

As stated in the introduction, LC molecules with certain shape asymmetry can result in the formation of splay-bend deformations in the LC director when subjected to an applied electric field. A three-dimensional coordinate system is employed to model the splay-bend distortion (illustrated in Fig. 1) whereby the z-axis is defined as the direction perpendicular to the plane of the glass substrates, effectively representing the thickness of the LC layer (d). The y-axis aligns with the initial alignment orientation, as shown in Fig. 1**(a)**, whereas the x-axis is the direction of the flexoelectric periodic splay-bend distortion. Two analytic models are used here. Firstly, a constrained approach is employed in this work which forces the alignment of the LC director to be within a conical structure, as depicted in Fig. 1**(b).** In addition, an unconstrained approach is also adopted to allow for the independent variation of the out-of-plane and in-plane tilt of the director, as demonstrated in Fig. 1**(c)**. Here, we define the pitch (p) as the distance for which there is one complete 2π period of the director reorientation.

(a) Unconstrained model

Bobylev and Pikin employed a model analogous to the unconstrained version, as referenced in [33]. The situation of small undulations was considered, where the magnitudes of $|\theta|$ and $|\varphi|$ are much less than 1; this condition significantly simplifies the computational process. For completeness, we now summarize the key findings from Ref. [33] and identify the conditions when the Fréedericksz threshold voltage and the threshold voltage for flexoelectric instability are the same. This enables us to distinguish when either dielectric coupling or flexoelectric coupling dominates.

In the small undulation scenario, where $|\theta|$, $|\varphi| \ll 1$, the LC director for unconstrained perturbations can be defined as follows:

$$\mathbf{n} = \begin{pmatrix} \cos\theta\sin\varphi \\ \cos\theta\cos\varphi \\ \sin\theta \end{pmatrix} \approx \begin{pmatrix} \varphi \\ 1 \\ \theta \end{pmatrix} \tag{1}$$

The interaction between the dielectric energy, flexoelectric energy, and elastic energy influences the orientation of the LC director. Assuming the Frank elastic constants are equal, and $\mathbf{E} = \begin{pmatrix} 0 \\ 0 \\ E \end{pmatrix}$ is the electric field applied along the z-axis, the total free energy can then be recast as

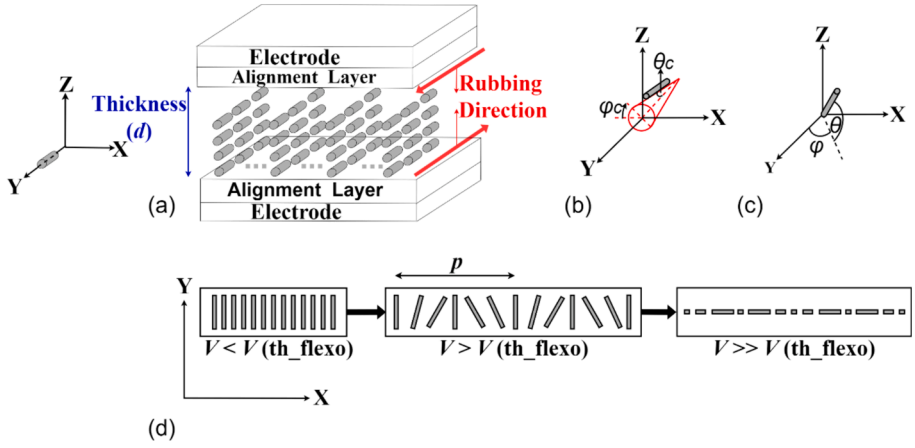

Fig. 1. (a) Initial alignment in an anti-parallel rubbed homogeneous LC glass cell without an applied voltage. (b) Constrained perturbation of the LC director in a conical configuration, with one end anchored at the base circumference and the opposite end directed towards the vertex. (c) Unconstrained perturbation of the LC director in the coordinate system. (d) Approximate top-view representation of the evolution of the LC director in the presence of flexoelectric coupling for different applied voltages. $V_{(\text{th\_flexo})}$ represents the threshold voltage to trigger the flexoelectric effect.

$$f = f_{elastic} + f_{flexoelectric} + f_{dielectric} \tag{2}$$

$$= \frac{1}{2}K\left\{[\nabla \bullet \mathbf{n}]^2 + [\nabla \times \mathbf{n}]^2\right\} - (e_1\mathbf{n}(\nabla \bullet \mathbf{n}) + e_3(\nabla \times \mathbf{n}) \times \mathbf{n}) \bullet \mathbf{E} - \frac{1}{2}\varepsilon_0\Delta\varepsilon(\mathbf{n} \bullet \mathbf{E})^2 \tag{3}$$

Minimizing the free-energy with respect to θ and φ necessitates the application of the Euler-Lagrange equations. By accounting for the boundary conditions, $\theta = \varphi = 0$ at $z = 0$ and $z = d$ (where d represents the thickness of the LC layer) and using the Euler-Lagrange equations, we can derive an expression for the electric field as a function of the wavenumber, q, of the periodic structure ($q = 2\pi/p$, where p is the pitch of the splay-bend structure). This takes the form

$$E^2 = \left(\frac{K}{e_1 - e_3}\right)^2 \frac{\left[q^2 + \left(\frac{\pi}{d}\right)^2\right]^2}{q^2 + \mu[q^2 + \left(\frac{\pi}{d}\right)^2]} \tag{4}$$

where $\mu = \frac{\Delta\varepsilon\varepsilon_0 K}{(e_1 - e_3)^2}$. It should be noted, however, that Eq. (4) is only valid at the threshold voltage where the director starts to reorient to form the splay-bend structure, therefore this equation defines the threshold field above which a non-trivial splay-bend modulation takes place. This is because the equation has been derived from the Euler-Lagrange equations using the small angle approximation and perturbation solution. The derivation process from Eqs. (1) to (4) is detailed in the Supplementary Information (Supplementary Information S1).

The threshold voltage for flexoelectric instability can be ascertained by examining the minimum electric field at $q = q_{th}$. By setting $\frac{d(E^2)}{dq} = 0$, we get

$$V_{(\text{th\_flexo})} = \frac{2\pi K}{(e_1 - e_3)(1 + \mu)} \tag{5}$$

$$q_{th} = \frac{\pi}{d}\sqrt{\frac{1 - \mu}{1 + \mu}} \tag{6}$$

In our LC tunable grating device, we anticipate a predominant flexoelectric effect, which is expected to facilitate more precise control over the alignment of the LC director. Nevertheless, it is also essential to investigate the impact of dielectric anisotropy on the formation of the gratings. According to Eq. (6), the flexoelectric instability can only occur if $|\mu| < 1$, which suggests that for a periodic flexoelectric structure to form we require

$$|\Delta\varepsilon| < \frac{(e_1 - e_3)^2}{K\varepsilon_0} \tag{7}$$

The threshold voltage to cause the Fréedericksz transition is calculated as $V_{(\text{th\_frkz})} = \pi\sqrt{\frac{K}{\Delta\varepsilon\varepsilon_0}}$. If $\mu = 1$, $\Delta\varepsilon = \frac{(e_1 - e_3)^2}{K\varepsilon_0}$ and thus $V_{(\text{th\_flexo})} = \frac{2\pi K}{(e_1 - e_3)(1+\mu)} = \frac{2\pi K}{\sqrt{K\varepsilon_0 * \Delta\varepsilon * (1+1)}} = \pi\sqrt{\frac{K}{\Delta\varepsilon\varepsilon_0}}$, which implies that $V_{(\text{th\_flexo})} = V_{(\text{th\_frkz})}$ when $\mu = 1$. Table 1 considers the dominant form of coupling for different magnitudes of $|\Delta\varepsilon|$ relative to the flexoelectric coefficients.

Table 1
Coupling regimes for the flexoelectric LC grating for different magnitudes of the dielectric anisotropy relative to the flexoelectric coefficients.

Relative magnitudes	Coupling mechanism
$\lvert\Delta\varepsilon\rvert \ll \frac{(e_1 - e_3)^2}{K\varepsilon_0}$	Flexoelectric coupling dominates
$\lvert\Delta\varepsilon\rvert \gg \frac{(e_1 - e_3)^2}{K\varepsilon_0}$	Dielectric coupling dominates
$\lvert\Delta\varepsilon\rvert \approx \frac{(e_1 - e_3)^2}{K\varepsilon_0}$	Flexoelectric coupling and dielectric coupling co-exist

(b) Constrained Model (Conical Model)

For the conical model, as first proposed by Shin [34], θ_c represents the angle at which the LC director tilts out of the axis of the cone whereas φ_c represents the rotation angle around the cone. Subsequently, a constrained model was constructed as shown in Fig. 1**(b)**. The model assumes a smooth rotation of the LC director along the x-axis to form a flexoelectric periodic splay-bend structure within the cone. Consequently, we can define $\varphi_c = qx$, where q represents the wavenumber as previously discussed. The LC director can thus be expressed in the small angle approximation as

$$\mathbf{n} = \begin{pmatrix} \sin\theta_c\cos\varphi_c \\ \cos\theta_c \\ \sin\theta_c\sin\varphi_c \end{pmatrix} \approx \begin{pmatrix} \theta_c\cos(qx) \\ 1 \\ \theta_c\sin(qx) \end{pmatrix} \tag{8}$$

Linking the above to the unconstrained model we get

$$\varphi = \theta_c\cos(qx) \text{ and } \theta = \theta_c\sin(qx) \tag{9}$$

Considering the strong surface anchoring ($\theta = 0$ at $z = 0$ and $z = d$), θ can be treated as a z-dependence sine-like perturbation, similar to that when deriving the Fréedericksz threshold in a nematic LC. We thus propose the form $\theta_c = \theta_0\sin\left(\frac{\pi z}{d}\right)$ where $\theta_0 \ll 1$. Inserting Eq. (9) into the free-energy equation (Eq. (3)) and then simplifying through integration, we obtained a reduced form of the free-energy as

$$< f >= \frac{K}{4}\theta_0{}^2\left(\frac{\pi^2}{d^2} + q^2\right) - \frac{q}{4}\theta_0{}^2(e_3 - e_1)E - \frac{1}{8}\varepsilon_0\Delta\varepsilon E^2\theta_0^2 \tag{10}$$

The minimization of $< f >$ can be achieved by setting $\frac{\partial < f >}{\partial q} = 0$. The last term containing $\Delta\varepsilon$ will not contribute to the derivation since it lacks dependence on q, thereby excluding dielectric components from the free-energy equation. We can then obtain an expression for the pitch of the periodic splay-bend structure as a function of the material properties and the electric field, as well as the threshold voltage required to trigger the flexoelectric-induced distortion. Respectively, these equations take the form

$$p = \frac{4\pi K}{E(e_3 - e_1)} \tag{11}$$

$$V_{(th\_flexo)} = \frac{2\pi K}{(e_3 - e_1)} \tag{12}$$

Compared to Eqs. (5) and (6), Eqs. (11) and (12) present a more simplified form by omitting the dielectric coupling. Furthermore, Eq. (11) yields the same results as those obtained from a different model, described in Ref [35], under the assumption that the elastic constants for splay and bend are equal.

(c) Nonlinear model

In the above linear analytic models, the small angle approximation has been employed to simplify the mathematical analysis. However, the application of the small angle approximation limits the validity of the resulting equations to scenarios with small undulations, thereby potentially compromising its accuracy in representing the LC director's actual behaviour in most nematic LC mixtures. Therefore, a nonlinear model that negates the need for the small angle approximation would be desirable. To accomplish this, we propose eliminating these simplifications and incorporating the complete unconstrained form of the LC director $\mathbf{n} = \begin{pmatrix} \cos\theta\sin\varphi \\ \cos\theta\cos\varphi \\ \sin\theta \end{pmatrix}$ directly in the total free-energy equation.

After employing the Euler-Lagrange equations to minimize the free energy with respect to the variables θ and φ, we obtain the following set of equations.

$$f_2(\varphi,\theta)=\frac{\partial^2\varphi}{\partial x^2}+\frac{\partial^2\varphi}{\partial z^2}-\frac{(e_1-e_3)E\cos(\varphi)}{K}\frac{\partial\theta}{\partial x}-2\tan(\theta)\left(\frac{\partial\theta}{\partial x}\frac{\partial\varphi}{\partial x}+\frac{\partial\varphi}{\partial z}\frac{\partial\theta}{\partial z}\right)=0 \tag{13}$$

$$g_2(\theta,\varphi)=\frac{\partial^2\theta}{\partial x^2}+\frac{\partial^2\theta}{\partial z^2}+\frac{(e_1-e_3)\cos(\varphi)(\cos(\theta))^2E}{K}\frac{\partial\varphi}{\partial x}+\frac{\varepsilon_0\Delta\varepsilon\cos(\theta)\sin(\theta)E^2}{K}+\cos(\theta)\sin(\theta)\left(\left(\frac{\partial\varphi}{\partial x}\right)^2+\left(\frac{\partial\varphi}{\partial z}\right)^2\right)=0 \tag{14}$$

The comprehensive derivation process to obtain Eqs. (13) and (14) is can be found in the Supplementary Information (Supplementary Information S2). The above two equations, which represent the stationary orientation of the LC director in the presence of flexoelectric coupling, contain additional terms that do not appear when the form of the LC director follows that of Eq. (1). It can be seen in Eq. (13) that $\frac{(e_1-e_3)E\cos(\varphi)}{K}\frac{\partial\theta}{\partial x}$ becomes the dominant factor when the LC is subjected to large voltages. Consequently, the contributions from the other terms can be considered negligible. Therefore, for the condition of $\frac{(e_1-e_3)E\cos(\varphi)}{K}\frac{\partial\theta}{\partial x}=0$, $\cos(\varphi)$ should be equal to zero. This implies that φ must be either $-\pi/2$ or $\pi/2$, which suggests that the LC director, due to the combined influence of the flexoelectric and dielectric coupling, tends to orient in the x-z plane, with little tilting in the x-y plane when extremely high voltages are applied, as shown in Fig. 1(d).

3. Simulations

To solve the partial differential equations (PDEs) obtained from the model described in the previous section and to understand the variations in θ and φ with respect to the spatial coordinates, it is necessary to implement a finite difference relaxation method; the methodology used in this work is presented in the Supplementary Information (Supplementary Information S3). For the simulations, values for macroscopic parameters such as the one elastic constant (K), splay flexoelectric coefficient (e_1), bend flexoelectric coefficient (e_3), dielectric anisotropy ($\Delta\varepsilon$), and refractive indices (n_e, n_o) of our LC mixture (*vide infra*) consisting of MLC6882 (Merck KGaA), BL006 (Merck KGaA), and CB7CB were taken from the following Refs. [29,36–39], where the relative concentrations of each component were taken into account to make reasonable and sensible estimates of the key material parameters of our mixture. Specifically, the elastic constant was assigned a value of K=13 pN, the dielectric anisotropy ($\Delta\varepsilon$) was set to $\Delta\varepsilon = 0.01$, and the extraordinary refractive index (n_e) was set at 1.594. In contrast, the ordinary refractive index (n_o) was chosen to be 1.487, and the effective flexoelectric coefficient was $e^* = e_1 - e_3 = 5.5\,\mathrm{pC/m^2}$, which falls within the first regime of Table 1.

According to Eq. (12), the threshold voltage required to trigger a flexoelectric response $V_{(\mathrm{th\_flexo})}$ was calculated to be 14.85 V and is found to agree well with our experimental results, which will be discussed in the following section. All simulation results presented in this paper are based on these estimated mixture parameters. However, the actual value of e^* and $\Delta\varepsilon$ might be higher than the estimations provided here because the application of the DC field can lead to the formation of ionic screening, which reduces the internal electric field and is not consistently controllable. Therefore, it is important to note that our simulations have not taken into account the influence of ions on the resultant behaviour. Examples of simulated LC director profiles for a range of applied voltages are shown in Fig. 2.

As illustrated in Fig. 2, when the applied voltage is below the threshold voltage, the LC director remains unchanged with uniform alignment along the y-axis, which is the direction of the initial alignment. Once the applied voltage exceeds the threshold voltage, the LC director exhibits a splay-bend structure within the x-z plane. Meanwhile,

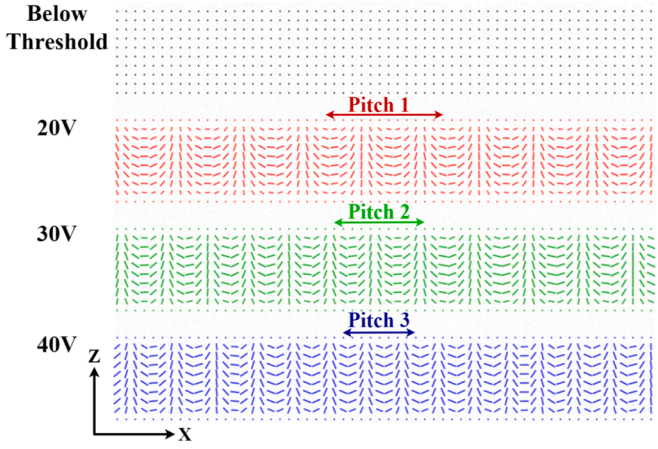

Fig. 2. Simulated voltage-dependent director profile and splay-bend structures formed in a nematic LC when viewed in the x-z plane for the following parameters: pre-tilt angle, $T_s = 0.05$ rad, K=13 pN, $e^* = 5.5\ \mathrm{pC/m^2}$, $d = 5\mu\mathrm{m}$ and $\Delta\varepsilon = 0.01$.

as the voltage increases, the pitch decreases proportionally, which is consistent with Eq. (12). The variations in θ and φ along the x-axis are illustrated, as detailed in the Supplementary Information (Supplementary Information S4).

To further study the behaviour of the LC director under the influence of flexoelectric coupling, both side and top views of the director profile were simulated using our nonlinear model (see Fig. 3). When the applied voltage is below the threshold, the LC director exhibits uniform alignment, parallel to the y-axis and predominantly lying within the x-y plane. However, once the applied voltage increases above the threshold voltage, it causes a gradual tilting of the director in both the x-y and x-z planes due to the combined influence of flexoelectric and dielectric effects. Under very strong electric field strengths, the LC director exhibits a predominant tilt in the x-z plane, with negligible tilt in the x-y plane. These simulation results align with the expected behaviour suggested in Fig. 1**(d)**.

Fig. 3**(c)** shows the average cone angle, determined by $\theta_c = \mathrm{acos}(n_y)$ where n_y is equal to $\cos(\theta)\cos(\varphi)$, as a metric to quantify the degree of tilt away from the y-direction. In the figure, D indicates the distance between the substrate surface of the device and the depth within the LC layer. It indicates that as the voltage increases above the threshold, the cone angle becomes more pronounced towards the middle of the layer, which is also observable in the side view profile.

Jones matrices were then employed to analyze light propagation through the flexoelectric LC gratings. The interplay of the flexoelectric and dielectric effects induces variability of the out-of-plane tilt angle, θ, along both the x-axis and z-axis, significantly influencing the variation in the effective refractive index experienced by light along the x and y-directions. Additionally, the in-plane tilt angle (φ) within the x-y plane varies along the x-axis due to the flexoelectric effect. The Jones matrix formulation is presented in Supplementary Information (Supplementary Information S3).

To simulate crossed polarized optical microscope images to compare with those from experiments, the CIE 1931 colour space [40] was employed. Central to this colour space is the colour-matching functions $\bar{x}(\lambda)$, $\bar{y}(\lambda)$, and $\bar{z}(\lambda)$, which span the wavelength range from 360 nm to 830 nm. These functions quantify the eye's response to different wavelengths of light, with $\bar{x}(\lambda)$ corresponding to the sensitivity to red light, $\bar{y}(\lambda)$ to green light, and $\bar{z}(\lambda)$ to blue light. As light interacts with the LC layer, it undergoes changes in the polarization, resulting in unique colour manifestations. The derivation of the XYZ tristimulus values was calculated by integrating over the wavelength from 360 nm to 830 nm. This integration involves the multiplication of $\bar{x}(\lambda)$, $\bar{y}(\lambda)$, and $\bar{z}(\lambda)$ colour

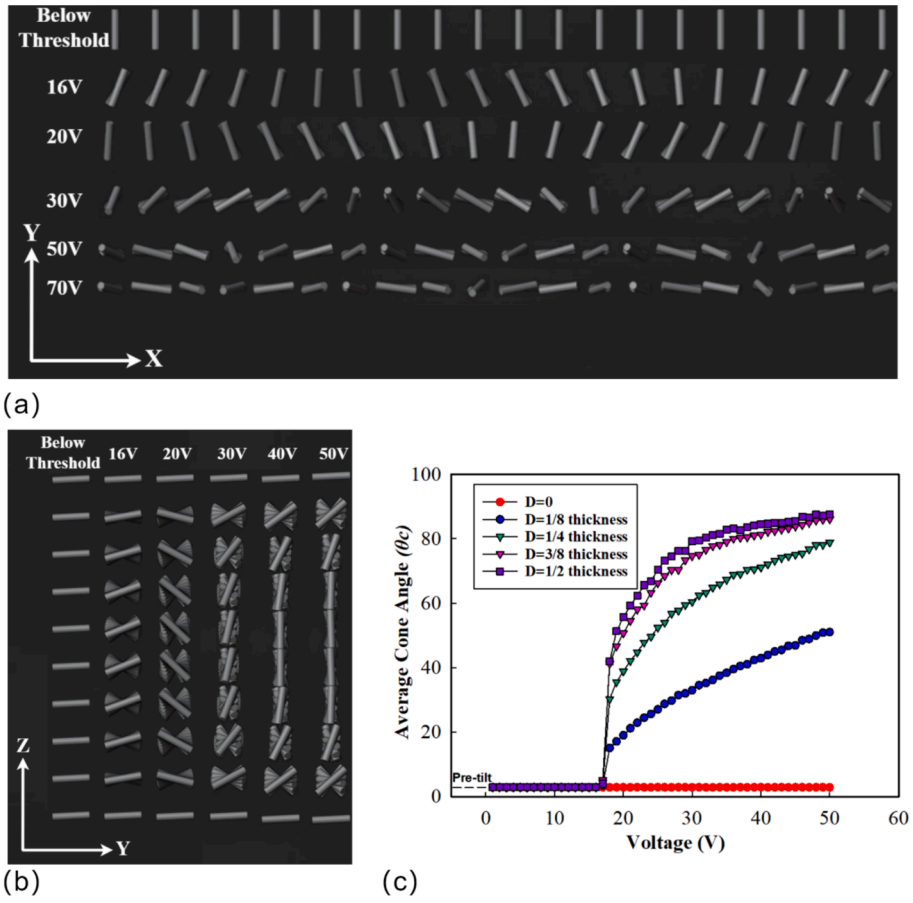

Fig. 3. (a) Simulated top view of the LC director profile for different applied voltages, specifically within LC layer depths (D) ranging from $D = \frac{2}{9}d$ to $D = \frac{7}{9}d$ (i.e., excluding the strongly anchored surface regions). (b) Simulated side view of the LC director profile for different applied voltages, with the presence of a surface anchoring layer. (c) Simulations of the variation of the average conical angle ($\theta_c = \text{acos}(n_y)$) at different depths ($D$) within the LC layer. The simulations were conducted using the following parameters: K=13 pN, $e^* = 5.5$ pC/m^2, $\Delta\varepsilon = 0.01$, $d = 5$μm, T_s= 0.05 rad.

matching functions, the transmittance properties of the LC material, and the D65 spectral power distribution, which simulates a standard daylight illuminance [40]. These XYZ tristimulus values were then transformed into RGB values through a matrix specific to the observing device's RGB colour space. Example results are presented later in Fig. 4 **(b)**.

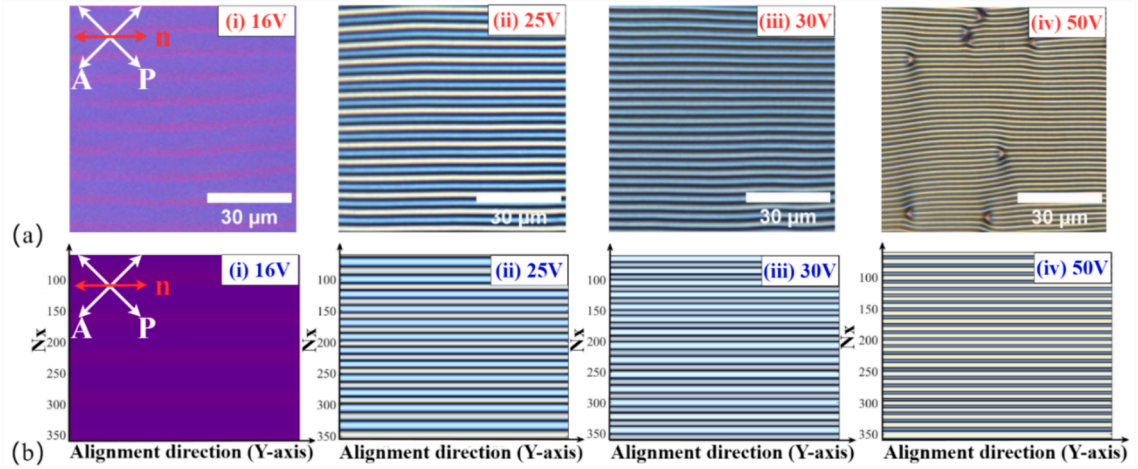

Fig. 4. Comparative analysis of polarized optical microscope images for different applied DC voltages: (i) 16 V, (ii) 25 V, (iii) 30 V, and (iv) 50 V: experimental data (a) at a temperature of 23℃ and the corresponding simulations (b) for the parameters K=13 pN, e^*= 5.5 pC/m^2, $\Delta\varepsilon = 0.01$, $d = 5$μm, n_e=1.594, n_o=1.487, $N_z = 40$, $N_x = 400$. N_x and N_z were employed in the numerical simulations to represent the number of grid points along the x-axis and the number of grid points across the thickness of the liquid crystal (LC) layer, respectively. The white double-headed arrows represent the polarizer (P) and analyzer (A) while the red double-headed arrowrepresents the alignment direction (**n**) of the LC director. The experiments were carried using an LC mixture composed of 81 wt% MLC-6882, 9 wt.% BL006, and 10 wt.% CB7CB with an LC layer thickness of 5 μm. Images were taken at a temperature of 23 °C.

We also simulated the normalized transmitted light intensities (η) in the far field, which is defined as the ratio of the intensity of light after passing through the LC grating under an applied voltage to the intensity of light without the LC grating (I_0) or when no voltage was applied to the LC grating. MATLAB's Fourier transform functionality was employed to convert the near-field output electric field ($E_{\text{near\_field}}$) into the far-field intensity distribution ($E_{\text{far\_field}}$). The intensity of light at the far field was calculated using the formula $I_{\text{out}} = |E_{\text{far\_field}}|^2$, and the initial light was computed as $I_{\text{in}} = |E_0|^2$, where E_0 represents the incident electric field. Consequently, the normalized light intensities of the LC grating were derived from the ratio of these two intensities, formulated as $\eta = I_{\text{out}}/I_{\text{in}}$. Then, the spatial frequencies (f_x) of the diffraction orders obtained from the Fourier transform were converted to diffraction angles (δ) using the relation $\delta = \sin^{-1}(\lambda f_x)$. The physical distance along the screen can then be simulated using the expression $L\tan(\delta)$, where L is defined as the distance between the screen and the LC device. The simulated normalized light intensities (η) as a function of distance on the screen from the zero order is shown in Fig. 5. Lastly, Fig. 7 presents the simulation results for the normalized light intensity at zero order.

4. Materials and methods

For the fabrication of a flexoelectric LC diffraction grating, our primary material of choice was the Synthon-sourced LC dimer CB7CB (4′,4″-(Heptane-1,7-diyl) dibiphenyl-4-carbonitrile). This dimer is composed of two cyanobiphenyl parts linked by a seven-carbon spacer. CB7CB is an exemplary candidate for flexoelectric applications as it exhibits a significant flexoelectric coefficient, reported to be approximately −31 pC/m [41]. Additionally, the dielectric anisotropy of CB7CB is quantified to be $\Delta\varepsilon = +2$ [37], which is low compared to more conventional nematic LCs. As discussed, a low dielectric anisotropy is advantageous for promoting the dominance of the flexoelectric effect. However, CB7CB exhibits a nematic phase within the temperature range of 105 °C–114 °C.

To obtain a nematic phase at room temperature, CB7CB needs to be mixed with other LC mixtures. For this purpose, we selected the wide temperature range nematic mixture, BL006. The downside is that BL006 has a relatively high dielectric anisotropy of +17.3 [26], which is not conducive to the flexoelectric properties required for our device. To reduce the overall dielectric anisotropy close to zero, we introduced a

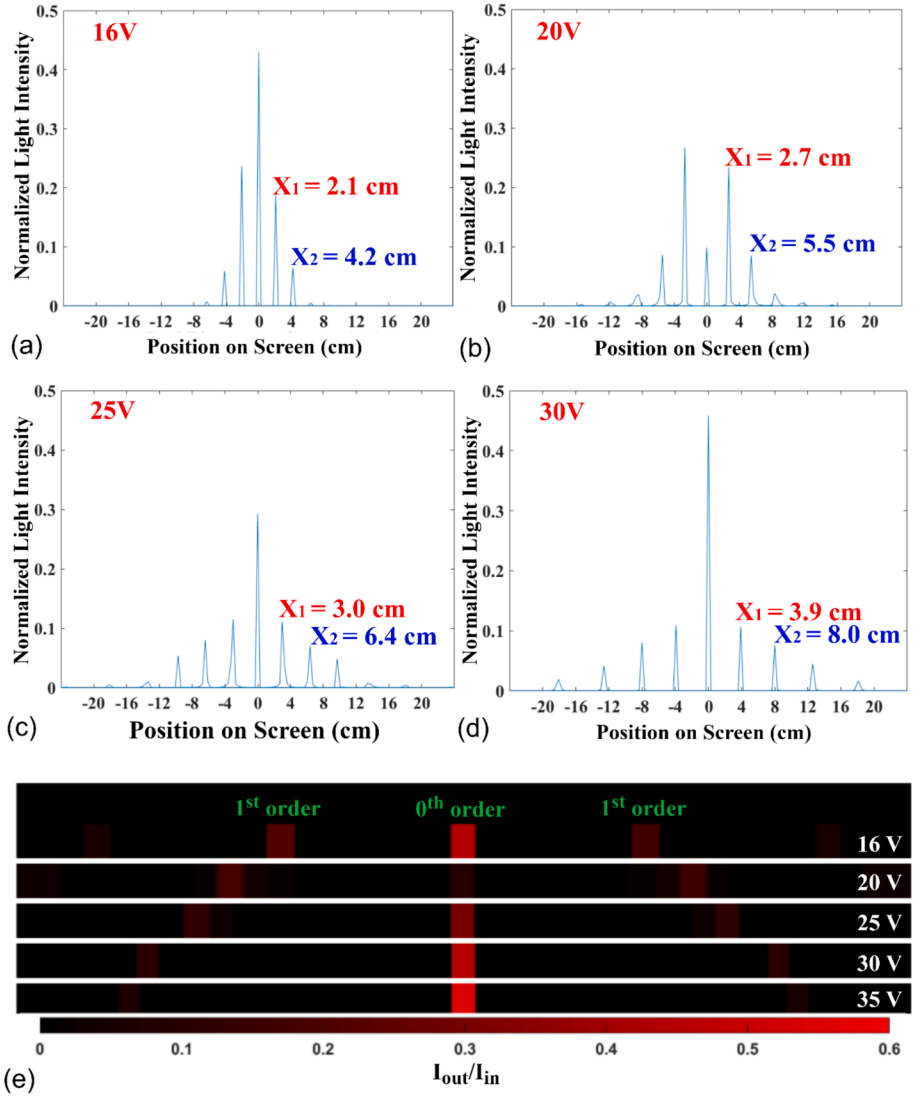

Fig. 5. (a)-(d) Simulated light intensity distribution in the far-field diffraction pattern, showing the normalized light intensities (η) as a function of distance on the screen from the 0th order. (e) Simulated diffraction patterns (0th order and 1st order) of the flexoelectric LC grating under various applied voltages, the colour bar is located at the bottom of the figure. The simulations were conducted using the following parameters: K=13 pN, e^* = 5.5 pC/m^2, n_e = 1.594, n_o = 1.487, $\Delta\varepsilon$ = 0.01, T_s = 0.05 rad. The incident linear polarization angle was set as $\alpha = 30^\circ$, and the distance between the screen and the LC device (L) was set at 30 cm.

substantial proportion of MLC-6882 (Merck KGaA) into the mixture. The dielectric anisotropy of MLC-6882 was found to be $\Delta\varepsilon \approx -2.82$. Through iterative optimization, we have developed an LC mixture comprising 81 wt% MLC-6882, 9 wt.% BL006, and 10 wt.% CB7CB. It remains in the nematic phase at room temperature and has a nematic-isotropic transition temperature of 80 °C. This mixture composition was filled into a 5 μm glass cell (INSTEC) via capillary action in the isotropic phase. The glass cell consisted of indium tin oxide (ITO) transparent electrodes coated onto the inner surfaces of the substrates onto which was coated a rubbed polyimide alignment layer. Glass spacer beads dispersed throughout the cell defined the thickness of the LC layer.

A polarizing optical microscope (BX51, Olympus) equipped with crossed polarizers and a CCD camera (R6, QImaging) mounted in the phototube was used to capture microphotographs of the gratings. A voltage was applied to the LC layer via a function generator that was connected to a voltage amplifier. To observe the diffraction pattern formed by the LC flexoelectric gratings, a PL202 laser diode ($\lambda = 639$ nm, Thorlabs) was employed as the coherent light source and a Neutral-Density (ND) Filter was used to attenuate the intensity to avoid saturation of the photodiode. A linear polarizer was placed before the LC grating to analyse the dependence of the flexoelectric grating on the incident polarization. Diffraction patterns were displayed on a white screen and captured using a CCD camera. The schematic of the optical setup for observing the diffraction is shown in Supplementary Information (Supplementary Information S5).

5. Results and discussion

(a) Polarized Optical Microscope Imaging

For our experimental investigation, the diffraction grating only exists within a notably narrow frequency range, up to 1.5 Hz, when an AC field is applied, due to the relatively large viscosity of the LC at room temperature. Furthermore, an AC field was found to facilitate the onset of electrohydrodynamic instabilities [42], which arise predominantly due to the periodic motion of ions. Consequently, all subsequent experiments were conducted using a DC field, which is considered more beneficial for ensuring the stability of the system at room temperature. The flexoelectric grating was found to operate over the temperature range of 20 °C–28 °C. In higher temperature ranges within the nematic phase, the diffractive effect is substantially reduced. This may be due to a decrease in the flexoelectric coefficients or changes in dielectric anisotropy at these temperatures. Additionally, at higher temperatures, ionic mobility increases, which also degrades the stability of the diffractive structures.

Fig. 4 presents observations of LC diffraction gratings on a crossed polarized optical microscope at a temperature of 23 ℃. The microscope stage was rotated to align the rubbing direction at a 45° angle relative to the polarizer and analyzer. Below the threshold voltage, no grating was observed. The threshold voltage required to observe the formation of a grating across the whole electrode region was found to be 15.5 V, which is close to the value of $V_{(\text{th\_flexo})}$, obtained from Eq. (12). As illustrated in Fig. 4**(a)**, exceeding the threshold voltage initiates a transformation into a striped appearance whereby the pitch of the LC grating narrows with increasing voltage, leading to a variation in the colour of the stripe. This colour change results from differential tilting and orientation of the LC director under varying voltage amplitudes. Fig. 4**a(iv)** shows the dislocations, which emerge as the system transitions to a higher voltage regime. Fig. 4**(b)** displays the outcomes of simulations employing our unconstrained nonlinear model, which use the CIE1931 colour space and Jones matrices to simulate light propagation when the grating is positioned between crossed polarizers on an optical microscope. The agreement between the predicted and observed grating patterns confirms the accuracy of our model and the computational techniques used. Additional microscope images corresponding to various applied DC voltages can be found in the Supplementary Information (Supplementary Information S6).

Table 2 shows a comparative analysis of the pitch of our mixture at different voltages obtained using three different methods. The three different methods include the predicted values, obtained from Eq. (11), the results from the nonlinear model numerical simulations, and the experimental observations. It can be seen that they exhibit a high degree of congruence and are in very good agreement, demonstrating a strong correlation between the theoretical analytical predictions, nonlinear numerical simulations, and experimental findings.

(b) Diffraction patterns

Fig. 5 presents the simulated intensity distribution and analytical diffraction patterns at various applied voltages using our nonlinear model. The results demonstrate that the spatial distance between each diffraction order increases with the applied voltage (Fig. 5(a)–(d)). X_1 represents the separation between the 0th and 1st order whereas X_2 denotes the separation between the 0th and 2nd order. However, the peaks in the distribution are not infinitely narrow and, consequently, do not exhibit δ-function characteristics because the numerically simulated splay-bend structure is not perfectly periodic. Additionally, the 0th-order normalized light intensity, as defined in Section 3, varies in response to different applied voltage amplitudes. These effects are also clearly visualized in Fig. 5(e), where the increase in separation between orders as the voltage increases can be clearly seen.

In this paper, the incident polarization angle, denoted as α, defines the orientation of the polarization with respect to the rubbing direction (y-axis) of the LC glass cell. Fig. 6 presents the results from experiments for the far-field diffraction patterns of light diffracted from our flexoelectric LC gratings when $\alpha = 30^{\circ}$. In accordance with the simulations, the results from the experiments show that the spacing between neighbouring diffraction orders increases as the voltage is increased, which results from a decrease in the pitch as the voltage is increased. In addition, it is evident that when the applied voltage is close to the threshold value ($V_{(\text{th\_flexo})}$, approximately 16 V in this case), the intensity of light in the 0th order is high, indicating weak diffraction. As the voltage increases from 18 V to 24 V, there is a noticeable decrease in the 0th order intensity, signifying a rise in diffraction. Beyond 24 V, the 0th order intensity starts to increase, implying a reduction in diffraction. This phenomenon is also shown in Fig. 7. This behaviour is described in more detail shortly.

Table 3 compares the separation of the diffraction orders in the far-field diffraction patterns for both the experiments and simulations at voltages ranging from 16 V to 35 V. For the 0th–1st order separation and 0th–2nd order separation, the numerical values obtained from experiments and simulations appear to be in good agreement, providing further evidence of the validity of our nonlinear model.

Replacing the screen with a photodiode allows the measurement of the normalized light intensities to be obtained. In this case, we focused specifically on the 0th order diffraction peak. The data presented in Fig. 7 includes results from simulations and experiments of the zero-order normalized light intensity as a function of the applied voltage for varying orientations of the incident linear polarization angle (α) ranging from 0 to 90°. It is observed that there is a critical turning point observable in each curve, after which the zero-order normalized light intensity either begins to increase sharply or approaches zero. Before the

Table 2
Comparative analysis of pitch values for a 5 μm thickness LC layer. Results from experiments, nonlinear numerical simulations (K=13 pN, $e^* = 5.5$ pC/m^2), and predictions based upon Eq. (11).

Applied Voltage (V)	20	25	30	35	40	45	50
Pitch (from Experiment (μm))	7.6	6.6	5.6	4.4	3.9	3.7	3.1
Pitch (from Simulations (μm))	7.2	6.3	5.5	4.5	4.0	3.3	3.0
$p = \frac{4\pi K}{E(e_3 - e_1)}$ (μm)	7.4	5.9	5.0	4.2	3.7	3.3	3.0

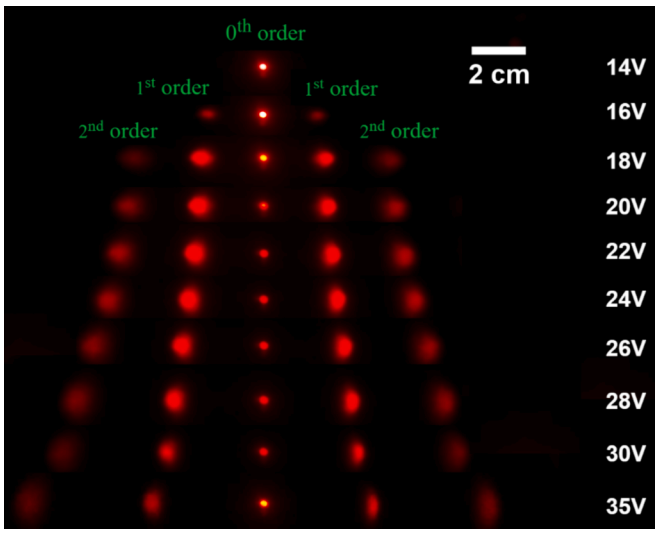

Fig. 6. Far-field diffraction patterns for the flexoelectric LC grating when illuminated with light from a laser diode and subjected to various applied voltages with the incident linear polarization angle set as $\alpha = 30^{\circ}$. The LC device was operated under the same conditions as described in Fig. 4.

turning point, there is a decrease in the 0th order normalized light intensity in each curve when the applied voltage exceeds the threshold ($V_{(th\_flexo)}$). The reduction in light intensity at the 0th order is caused by flexoelectric coupling, which leads to a tilt in both the *x*-*y* and the *x*-*z* planes, resulting in the diffraction of light.

The results show that the zero-order normalized light intensity approached zero at high voltages for an incident polarization angle of $\alpha = 90^{\circ}$, indicating that the light is diffracted into other orders, decreasing the intensity of the 0th order diffraction. It is interesting to note that this effect is due to the particular device thickness and LC optical anisotropy used in this work. Excluding the $\alpha = 90^{\circ}$ case, the zero-order normalized light intensity increases with applied voltage after the turning point. Larger polarization angles correlate with smaller increases in the zero-order normalized light intensity when the applied voltage is increased, which can be attributed to the behaviour of the LC director at high voltages as a result of flexoelectric coupling. As previously discussed, at very high voltages, the LC director tends to orient predominantly within the *x*-*z* plane, exhibiting a purely splay-bend alignment along the *x*-axis: this orientation significantly affects the interaction with polarized light.

When the polarization angle is set to 0°, aligning parallel to the *y*-axis (the rubbing direction of the LC glass cell), the incident polarized light only experiences the ordinary refractive index if the director is in the *x*-*z* plane. Under these conditions, at very high voltages, the light does not undergo significant diffraction, leading to a decrease in the intensity of light in the higher diffraction orders. Consequently, the intensity observed in the 0th order spot increases. Conversely, at a polarization angle of 90°, where the polarization direction is perpendicular to the *y*-axis, the polarized light interacts with the pure splay-bend profile aligned along the *x*-*z* plane, this interaction results in a periodic variation of the refractive index along the *x*-axis, effectively forming a phase grating. Such a configuration facilitates maximal diffraction of light, thereby reducing the light intensity observed in the 0th order light. These results reinforce the simulated director behaviour shown in Fig. 3.

6. Conclusions

In summary, we present both modelling and experimental investigations of flexoelectric-based diffraction gratings in nematic LCs. We start by considering a linear analytic model in which the tilt of the LC director is assumed to be small in both the unconstrained and constrained (conical) coordinate systems and investigate the influence of dielectric anisotropy on the behaviour of the grating. Subsequently, we present a nonlinear method that obviates the need for a small angle approximation and includes dielectric coupling to provide a more sophisticated model of flexoelectric LC gratings. Numerical simulations based upon this model provides important insight into the behaviour of the LC director as the grating forms and varies, facilitating the simulation of light intensity distribution in the far-field and the resulting diffraction pattern, as well as the grating's dependence on incident polarization using Jones matrices.

An LC mixture was developed, comprising 9 wt% BL006, 81 wt% MLC-6882, and 10 wt% CB7CB. This mixture, characterized by low dielectric anisotropy, exhibits the formation of a flexoelectric LC diffraction grating at room temperature (25 ℃) using a DC field ranging from 16 V to 50 V. The resulting grating has a pitch that ranges from 3 μm to 8 μm, depending upon the magnitude of the applied voltage.

Simulation and experimental results indicate that increasing voltage alters the director alignment from its initial state defined by the rubbing direction to a state where the director exhibits both in-plane (*x*-*y* plane) and out-of-plane (*x*-*z* plane) tilt. At very high voltages, a predominant tilt in the *x*-*z* plane is observed, with negligible tilt in the *x*-*y* plane. The 0th order light intensity confirms our predictions about the director

Table 3
Comparison of the separation of the different diffraction orders obtained from both experiments and simulations for five different applied voltages. The incident linear polarization angle $\alpha = 30^{\circ}$.

Applied Voltage (V)	0th–1st order separation (cm)		0th–2nd order separation (cm)	
	Experiment	Simulation	Experiment	Simulation
16	2.0	2.1	4.2	4.2
20	2.4	2.7	4.8	5.5
25	2.8	3.0	5.7	6.4
30	3.5	3.9	7.2	8.0
35	4.1	4.5	8.4	9.3

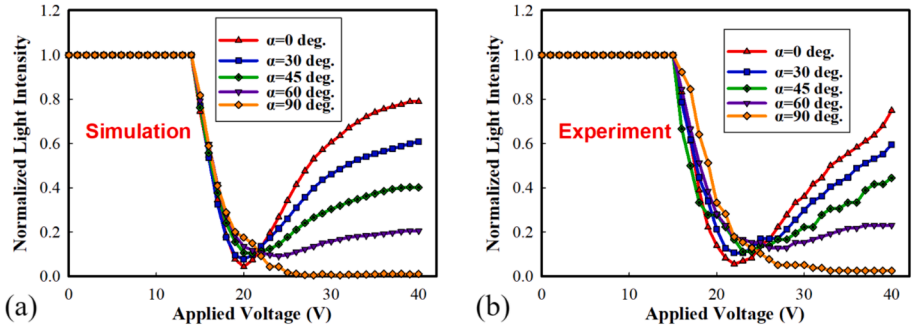

Fig. 7. Normalized light intensity of the 0th order as a function of the voltage applied to the LC grating. Results are presented for different orientations of the incident linear polarization. (a) Simulation and (b) experimental results for the same conditions as described in Fig. 4.

profile, and there is a strong similarity between our modelling and experimental results of the pitch of the grating with applied voltage and the light intensity at the far-field, thereby supporting the reliability of our model. Our nonlinear model greatly improves the predictability of flexoelectric LC gratings and aids in optimizing material design, which is of importance in the development of advanced display technologies, switchable holograms, and innovative beam-steering applications.

CRediT authorship contribution statement

Qihao Han: Conceptualization, Data curation, Formal analysis, Investigation, Writing – original draft. **Steve J. Elston:** Conceptualization, Formal analysis, Investigation, Methodology, Supervision, Writing – original draft. **Waqas Kamal:** Data curation, Formal analysis, Methodology, Project administration, Supervision, Writing – original draft. **Linpei Xue:** Formal analysis, Investigation, Writing – review & editing. **Stephen M. Morris:** Conceptualization, Funding acquisition, Project administration, Resources, Supervision, Writing – review & editing.

Declaration of competing interest

The authors declare the following financial interests/personal relationships which may be considered as potential competing interests: Stephen Morris reports financial support was provided by Engineering and Physical Sciences Research Council. If there are other authors, they declare that they have no known competing financial interests or personal relationships that could have appeared to influence the work reported in this paper.

Data availability

Data will be made available on request.

Acknowledgements

This research was funded in whole, or in part, by the Engineering and Physical Sciences Research Council (UK) [EP/W022567/1]. For the purpose of Open Access, the author has applied a CC BY public copyright licence to any Author Accepted Manuscript version arising from this submission.

Appendix A. Supplementary material

Supplementary data to this article can be found online at https://doi.org/10.1016/j.optlastec.2024.111502.

References

[1] R.F. Bryan, Electrooptic effects in liquid crystal materials by L. M. Blinov and V. G. Chigrinov, J. Appl. Cryst. 29 (1996) 6, https://doi.org/10.1107/s0021889896099517.
[2] D. Zhao, W. Bi, B.Z. Tang, A light-emitting liquid crystal display device without polarizers and alignment layers, Adv. Opt. Mater. 9 (2021) 19, https://doi.org/10.1002/adom.202100489.
[3] L.T. Creagh, A.R. Kmetz, R.A. Reynolds, Performance characteristics of nematic liquid crystal display devices, IEEE Trans. Electron Dev. 18 (1971) 9, https://doi.org/10.1109/T-ED.1971.17265.
[4] M. Jamil, F. Ahmad, J.T. Rhee, Y.J. Jeon, Nanoparticle-doped polymer-dispersed liquid crystal display, Curr. Sci. 101 (2011) 12.
[5] H.W. Chen, J.H. Lee, B.Y. Lin, S. Chen, S.T. Wu, Liquid crystal display and organic light-emitting diode display: present status and future perspectives, Light Sci. Appl. 7 (2018) 3, https://doi.org/10.1038/lsa.2017.168.
[6] Z. He, F. Gou, R. Chen, K. Yin, T. Zhan, S.T. Wu, Liquid crystal beam steering devices: principles, recent advances, and future developments, Crystals (Basel) 9 (2019) 6, https://doi.org/10.3390/cryst9060292.
[7] P. F. McManamon et al., A review of phased array steering for narrow-band electrooptical systems, in: Proceedings of the IEEE, vol. 97, 6. 2009. doi: 10.1109/JPROC.2009.2017218.
[8] J. Kim, C. Oh, M. J. Escuti, L. Hosting, S. Serati, Wide-angle nonmechanical beam steering using thin liquid crystal polarization gratings, in: Advanced Wavefront Control: Methods, Devices, and Applications VI, 2008. doi: 10.1117/12.795752.
[9] D.P. Resler, D.S. Hobbs, R.C. Sharp, L.J. Friedman, T.A. Dorschner, High-efficiency liquid-crystal optical phased-array beam steering, Opt. Lett. 21 (1996) 9, https://doi.org/10.1364/ol.21.000689.
[10] Y.L. Li, et al., Tunable liquid crystal grating based holographic 3D display system with wide viewing angle and large size, Light Sci. Appl. 11 (2022) 1, https://doi.org/10.1038/s41377-022-00880-y.
[11] K.A. Rutkowska, A. Kozanecka-Szmigiel, Design of tunable holographic liquid crystalline diffraction gratings, Sensors (Switzerland) 20 (2020) 23, https://doi.org/10.3390/s20236789.
[12] K. Wang, J. Zheng, Y. Liu, H. Gao, S. Zhuang, Electrically tunable two-dimensional holographic polymer-dispersed liquid crystal grating with variable period, Opt. Commun. 392 (2017), https://doi.org/10.1016/j.optcom.2017.01.030.
[13] R.K. Komanduri, C. Oh, M.J. Escuti, 34.4L: late-news paper: polarization independent projection systems using thin film polymer polarization gratings and standard liquid crystal microdisplays, SID Symposium Digest of Technical Papers 40 (2009) 1, https://doi.org/10.1889/1.3256822.
[14] I. Fujieda, Liquid-crystal phase grating based on in-plane switching, Appl. Opt. 40 (2001) 34, https://doi.org/10.1364/ao.40.006252.
[15] J.H. Park, C.J. Yu, J. Kim, S.Y. Chung, S.D. Lee, Concept of a liquid-crystal polarization beamsplitter based on binary phase gratings, Appl. Phys. Lett. 83 (2003) 10, https://doi.org/10.1063/1.1609042.
[16] J. Chen, P.J. Bos, H. Vithana, D.L. Johnson, An electro-optically controlled liquid crystal diffraction grating, Appl. Phys. Lett. 67 (1995), https://doi.org/10.1063/1.115140.
[17] J. Kim, J.-H. Suh, B.-Y. Lee, S.-U. Kim, S.-D. Lee, Optically switchable grating based on dye-doped ferroelectric liquid crystal with high efficiency, Opt. Exp. 23 (2015) 10, https://doi.org/10.1364/oe.23.012619.
[18] C.L. Tien, R.J. Lin, S.H. Su, C.T. Horng, Electrically tunable diffraction grating based on liquid crystals, Adv. Condens. Matter Phys. 2018 (2018), https://doi.org/10.1155/2018/7849529.
[19] S.Y. Huang, B.Y. Huang, C.C. Kang, C.T. Kuo, Diffraction and polarization properties of electrically-tunable nematic liquid crystal grating, Polymers (Basel) 12 (2020) 9, https://doi.org/10.3390/POLYM12091929.
[20] K. Gao, H.-H. Cheng, A.K. Bhowmik, P.J. Bos, Thin-film Pancharatnam lens with low f-number and high quality, Opt. Exp. 23 (20) (2015) 26086, https://doi.org/10.1364/oe.23.026086.
[21] K.G. Kamiak, O.S. Kabanova, I.I. Rushnova, E.A. Melnikova, A.L. Tolstik, Switchable diffraction gratings based on the periodic binary alignment of a nematic liquid crystal, Bull. Russ. Acad. Sci. Phys. 85 (2021) 12, https://doi.org/10.3103/S106287382112011X.
[22] J. Zhou, D.M. Collard, M. Srinivasarao, Switchable gratings by spatially periodic alignment of liquid crystals via patterned photopolymerization, Opt. Lett. 31 (2006) 5, https://doi.org/10.1364/ol.31.000652.
[23] A. Ryabchun, A. Bobrovsky, J. Stumpe, V. Shibaev, Rotatable diffraction gratings based on cholesteric liquid crystals with phototunable helix pitch, Adv. Opt. Mater. 3 (2015) 9, https://doi.org/10.1002/adom.201500159.
[24] W.C. Hung, I.M. Jiang, M.S. Tsai, P. Yeh, W.H. Cheng, Tunable cholesteric liquid crystal diffraction grating based on the effect of localized surface plasmons, in: Optics InfoBase Conference Papers, 2010, https://doi.org/10.1364/cleo.2010.ctug4.
[25] D. Subacius, S.V. Shiyanovskii, P. Bos, O.D. Lavrentovich, Cholesteric gratings with field-controlled period, Appl. Phys. Lett. 71 (1997) 23, https://doi.org/10.1063/1.120325.
[26] R. Hamdi, G. Petriashvili, M.P. De Santo, G. Lombardo, R. Barberi, Electrically controlled 1D and 2D cholesteric liquid crystal gratings, Mol. Cryst. Liq. Cryst. (2012), https://doi.org/10.1080/15421406.2011.609436.
[27] Y. Li, Z. Guo, Y.M. Zeng, L. Yu, L.L. Tian, F. Chu, Low voltage dual-period liquid crystal grating with tunable diffraction efficiency, Displays 80 (2023), https://doi.org/10.1016/j.displa.2023.102562.
[28] R.B. Meyer, Piezoelectric effects in liquid crystals, Phys. Rev. Lett. 22 (1969) 18, https://doi.org/10.1103/PhysRevLett.22.918.
[29] I. Dierking, Flexoelectricity in liquid crystals, Liq. Cryst. Today 22 (2013) 2, https://doi.org/10.1080/1358314x.2013.829929.
[30] Y. Xiang, et al., Tunable optical grating based on the flexoelectric effect in a bent-core nematic liquid crystal, Phys. Rev. Appl 7 (2017) 6, https://doi.org/10.1103/PhysRevApplied.7.064032.
[31] N. Éber, Y. Xiang, Á. Buka, Bent core nematics as optical gratings, J. Mol. Liq. 267 (2018), https://doi.org/10.1016/j.molliq.2017.09.025.
[32] M.-Y. Xu, M. Zhou, Y. Xiang, P. Salamon, N. Éber, Á. Buka, Domain structures as optical gratings controlled by electric field in a bent-core nematic, Opt. Exp. 23 (2015) 12, https://doi.org/10.1364/oe.23.015224.
[33] Yu. Bobylev, S. Pikin, Threshold piezoelectric instability in a liquid crystal, Soviet J. Exp. Theor. Phys. 45 (1977) 1.
[34] Y. Shin, Z. Zhou, S. Harder, X. Zhang, D.K. Yang, Reconfigurable liquid crystal diffraction grating based on flexoelectric effect, J. Mol. Liq. 357 (2022), https://doi.org/10.1016/j.molliq.2022.119150.
[35] L.A. Parry-Jones, R.B. Meyer, S.J. Elston, Mechanisms of flexoelectric switching in a zenithally bistable nematic device, J. Appl. Phys. 106 (2009) 1, https://doi.org/10.1063/1.3153971.

[36] A. Lorenz, et al., Electrical addressing of polymer stabilized hyper-twisted chiral nematic liquid crystals with interdigitated electrodes: experiment and model, Appl. Phys. Lett. 104 (2014) 7, https://doi.org/10.1063/1.4865558.
[37] G. Babakhanova, et al., Elastic and viscous properties of the nematic dimer CB7CB, Phys. Rev. E 96 (2017) 6, https://doi.org/10.1103/PhysRevE.96.062704.
[38] J. Li, G. Baird, Y. Lin, H. Ren, S. Wu, Refractive-index matching between liquid crystals and photopolymers, J. Soc. Inf. Disp. 13 (2005) 12, https://doi.org/10.1889/1.2150371.
[39] Y. Chen, F. Peng, T. Yamaguchi, X. Song, S.T. Wu, High performance negative dielectric anisotropy liquid crystals for display applications, Crystals 3 (2013) 3, https://doi.org/10.3390/cryst3030483.
[40] F.W. Billmeyer, H.S. Fairman, CIE method for calculating tristimulus values, Color Res. Appl. 12 (1987) 1, https://doi.org/10.1002/col.5080120106.
[41] A. Varanytsia, L.C. Chien, Giant flexoelectro-optic effect with liquid crystal dimer CB7CB, Sci. Rep. 7 (2017), https://doi.org/10.1038/srep41333.
[42] H. Gruler, Williams domains and dielectric alignment in a nematic liquid crystal, Mol. Cryst. Liq. Cryst. 27 (1974) 1–2, https://doi.org/10.1080/15421407408083118.